Environ Fluid Mech (2015) 15:1241–1262
DOI 10.1007/s10652-015-9412-5

ORIGINAL ARTICLE

Experimental study on growth and spread of dispersed particle-laden plume in a linearly stratified environment

Harish N Mirajkar[1] · Siddhesh Tirodkar[1] · Sridhar Balasubramanian[1]

Received: 2 December 2014 / Accepted: 18 April 2015 / Published online: 3 May 2015

Abstract We present results of laboratory experiments conducted to study the evolution, growth, and spreading rate of a dispersed particle-laden plume produced by a constant inflow into a density varying environment. Particles having mean size, $d_p = 100$ μm, density $\rho_p = 2500$ kg/m^3, volume fraction, $\phi_v = 0$–0.7 % , were injected along with the lighter buoyant fluid into a linearly stratified medium. It was observed that a particle-laden plume intruding at the neutral density layer is characterized by four spreading regimes: (i) radial momentum flux balanced by the inertia force; (ii) inertia buoyancy regime; (iii) fluid-particle inertia regime, and (iv) viscous buoyancy regime. Regimes (i), (ii), and (iv) are similar to that of a single-phase plume, for which $\phi_v = 0\,\%$. The maximum height, Z_m, for $\phi_v > 0\,\%$ was observed to be consistently lower than the single-phase case. An empirical parameterization was developed for the maximum height for particle-laden case, and was found to be in very good agreement with the experimental data. In the inertia buoyancy regime, the radial spread of the plume, R_f, for $\phi_v > 0\,\%$, advanced in time as $R_f \propto t^{0.68\pm0.02}$ which is slower compared to the single-phase plume that propagates at $R_f \propto t^{0.74\pm0.02}$. Due to the presence of particles, 'particle fall out' effect occurs, which along with the formation of a secondary umbrella region inhibits the spreading rate and results in slower propagation of the particle-laden plume. The effect of particles on spreading height of plume, Z_s, and thickness of the plume, h_p, were also studied, and these results were compared with the single-phase case. Overall from these experiments, it was found that the evolution, growth, and spread of dispersed particle-laden plume is very different from that of the single-phase plume, and presence of low concentration of particles ($\phi_v < 1\,\%$) could have significant effects on the plume dynamics.

Keywords Plume · Particles · Maximum height · Radial intrusion · Plume thickness

✉ Sridhar Balasubramanian
sridharb@iitb.ac.in

[1] Department of Mechanical Engineering, Indian Institute of Technology Bombay, Powai, Mumbai 400076, India

1 Introduction and previous work

Motions comprising of jets and plumes are ubiquitous in both environmental as well as engineering flows. Some examples include release of hot gases during volcanic eruptions, gravity currents, ocean overflows, and effluent discharges into water bodies. Such motions could also be associated with phase change as seen during cloud formation. These fluid motions are greatly modified in the presence of a stratified, density varying ambient environment [1–3]. In the presence of gravity, these density differences have a dramatic impact on the dynamics and mixing of heterogeneous fluids. For example, thermal stratification in reservoirs can reduce the vertical mixing of oxygen to the point that water at the bottom becomes anoxic through the action of biological processes. The Gulf oil spill disaster during the year 2010 is yet another instance where ocean stratification modified the dynamics of the oil-gas jet [4]. The complex nature of this problem coupled with numerous external flow factors renders the study of plume dynamics in stratified environment as an important underlying problem in many geophysical flows.

Near the source, the buoyant jet (or a forced plume) is momentum dominated, and as this forced plume evolves in space and time, it transitions to a pure plume that is dominated by buoyancy effects. Three different regimes were defined in a stratified environment, namely, (a) starting forced plume ($\lambda < 1$), (b) pure plume ($\lambda = 1$), and (c) lazy plume ($\lambda > 1$) where λ is the ratio of initial buoyancy flux B_0 to initial momentum flux M_0. The initial buoyancy flux and momentum flux are defined as follows [5],

$$B_0 = \frac{1}{4}\pi d_j^2 W_0 g\left(\frac{\rho_j - \rho_b}{\rho_b}\right) \tag{1}$$

$$B_0 = g\left(\frac{\rho_j - \rho_b}{\rho_b}\right) Q_0 = g' Q_0 \tag{2}$$

$$M_0 = Q_0 W_0 \tag{3}$$

$$Q_0 = \frac{1}{4}\pi d_j^2 W_0 \tag{4}$$

Here, d_j is the diameter of the jet, W_0 is the initial vertical velocity, ρ_j is the uniform density of the jet fluid, ρ_b is the density of bottom stratified layer, g is the gravity, $g' = g(\rho_j - \rho_b)/\rho_b$ is reduced gravity or buoyancy and Q_0 is the flow rate. Various external parameters, such as a steady mean flow or current, presence of particles in the plume fluid, and thermodynamic heating, to name a few could significantly modify the plume dynamics.

The single-phase plume (i.e. without any particles) behaviour in a stratified environment has been studied extensively in the past [6–10]. Experiments were initially done by Morton et al. [8] to measure the maximum height and validate it with an empirical formula. Most of the theory on plumes was based on a self-similarity analysis using the governing equations for stratified flows, namely conservation of mass, momentum and density deficiency along with the Boussinesq approximation [8]. In order to close the equations the entrainment assumption was introduced, which states that in a stably stratified ambient, the plume density increases steadily owing to entrainment, while that of the ambient fluid decreases steadily with height. The analysis proposed by Morton et al. [8] assumed that (i) rate of entrainment at edge of the plume is proportional to some characteristic velocity at that height, (ii) profiles of vertical velocity are self-similar at all heights, and (iii) the flow

satisifies Boussinessq approximation. Based on this, the mean horizontal entrainment velocity (u_e) was found to be proportional to the mean vertical velocity in the plume (W_c) at that height, i.e., $u_e = \alpha W_c$, where α is the entrainment coefficient. The entrainment coefficient, α can have varying values depending on the flow conditions, i.e., whether it is a jet, buoyant jet or pure plume. By using dimensional arguments, the maximum height, Z_m for such buoyant jets was related to the local buoyancy flux (B_0), the local momentum flux (M_0), and the Brunt Vaisala frequency, $N = \sqrt{\frac{-g}{\rho_b}\frac{\partial \rho}{\partial z}}$, where ρ_b is the bottom density of the linearly stratified fluid, and $\partial\rho/\partial z$ is the vertical density gradient [11]. The Brunt Vaisala frequency, N, is the frequency at which a fluid particle oscillates when displaced vertically within a stably stratified environment. In other words, N, governs the stability of the enviroment. Based on the flow parameters, the flow regimes could be defined using $(M_0/B_0)N^{1/2}$ as follows [12]: When $(M_0/B_0)N^{1/2} < 0.1$, the flow is a lazy plume for which $\alpha \approx 0.083$; for $0.1 < (M_0/B_0)N^{1/2} < 2$ the regime is termed buoyant jet or forced plume for which α varies based on the flow conditions; and for $(M_0/B_0)N^{1/2} > 2$, it is a jet flow for which $\alpha \approx 0.05$. Therefore, the entrainment of the discharged fluid with the ambient fluid depends on the flow regime defined based on M_0, B_0, and N. For plumes, the relation for Z_m is only dependent on buoyancy flux, B_0 and Brunt Vaisala frequency, N.

There are two basic approaches to calculating the value of α, namely, by measuring the radial growth of the plume, or by measuring the bulk parameter such as the maximum height Z_m, and then infering α from its predictions. It has been noted that the radial growth technique gives higher value of α compared to the bulk measurement method [13]. It should also be noted that the relations for Z_m are based on the similarity solutions, where a great deal of physics is hidden in the formula, but nevertheless works. Since the seminal work by Morton et al. [8], numerous researchers have studied the mixing and turbulence in stratified flows [1, 6, 14, 3, 15]. Some studies have also been conducted to capture the plume behavior in miscible fluids, e.g. oil and oil with surfactant [16]. The presence of mean flow on the single phase plume behavior showed that the mean flow increases the entrainment and the plumes becomes momentum dominated [17, 18]. In the last decade, turbulent mixing dynamics of buoyant jet and plumes have been addressed using state-of-the-art experimental measuring techniques such as particle image velocimetry (PIV) and planar laser induced fluorescence (PLIF) [5, 15]. The space and time evolution of turbulent quantities such as turbulent kinetic energy (K), Reynolds stress (R_{ij}), and buoyancy fluxes (B_i) are reported that are needed to fine tune the mixing length and turbulence models involving stratified fluids. Numerical study on single phase plume dynamics in uniform density environment has also been performed by various researchers [19–21].

Almost all the studies mentioned above have focused on the single-phase plume dynamics, where the effect of particles has been ignored. In principle, any geophysical and industrial flow (e.g. volcanic eruption, chimney exhaust) would have some concentration of solid particles in them [16, 22, 23]. The particle volume concentration could range anywhere from $\phi_v \approx 0.1$–30 %. The presence of high particle volume concentration is expected to change the plume dynamics drastically. However, not much is known when dispersed particle phase is present in the fluid ($\phi_v < 1$ %), where,

$$\phi_v = \frac{V_p}{V_p + V_f} \tag{5}$$

In Eq. (5), V_p is the particle volume, and V_f is the fluid volume. The study on particle-laden plume has significantly progressed in the last two decades, but we are still far from

completely understanding the plume dynamics in the presence of low/high particle concentrations. Reingold et al. [24] studied particle-laden plume in linearly stratified medium to model the bubble plume for varying particle diameter and determined the maximum height of the plume. Socolosky and Adams [18], studied multiphase plumes using particles and air bubbles in cross flow condition to study the separation height and trap height of plumes. Zarrebini and Cardoso [25, 26] conducted experiments where particle-laden plumes were released across density stratified medium. In their studies, continuous plume was positive buoyant containing negatively buoyant particles. The particles used were fine particles ($d_p < 100\,\mu m$) that were advected by the surrounding fluid, suggesting that $U_N \ll 1$ in the flow, where U_N is the non dimensional slip velocity, defined as the ratio of the particle terminal velocity to the characteristic plume fluid rise velocity [18]. Ernst et al. [27] conducted laboratory experiments using particle-laden fresh water rising through a tank filled with aqueous saline solution. They developed a model for sedimentation from radially spreading gravity currents generated by turbulent plumes, which showed good agreement with experimental data. Carey et al. [28] experimentally investigated the stability of particle-laden plumes as particle load was increased. Veitch and Woods [29] developed experiments to examine the effect of re-entrainment of particles on the spreading umbrella cloud. They injected fresh particle-laden water into the base of a tank of saline solution, with the particle load being sufficiently small that the fresh water led to the formation of a buoyant plume. As particles began to settle through the ambient fluid, some were gradually re-entrained into the plume, decreasing the buoyancy, until eventually, the mixture ceased to be buoyant and the plume collapsed upon itself. In the case of Zarrebini and Cardoso [25], the particles, while sinking back to the bottom were entrained towards the rising plume. As a result, the sediments or particles that were collected showed a distribution with zero sediment near the source region. Chow [30] experimentally studied the negative buoyant plume with positive buoyant particles to determine the maxium height of the plume by varying particle diameter. In their study, radial distribution of particles was also measured post experiments. Chan et al. [31] experimentally studied the radial distribution of particle-laden plume for different particle diameters and a theortical model was developed to validate the experimental results. Further, Jessop et al. [32] studied the effect of particles on the umbrella cloud or trapped plume, and found the effect of particles on the dynamics, stability and longevity of umbrella clouds. All these above mentioned studies have primarily focused on measuring the maximum height of the plume and particle distribution with or without cross flow in stratified conditions.

Inspite of the research progress in multi-phase plume behavior, the evolution, growth and spread of the plumes, and formation of umbrella cloud is not well understood, especially when dispersed particles are present in the plume. The main aim of the present work is to experimentally study and understand the effect of dispersed particle concentrations on the bulk flow parameters such as maximum height, spread height, spreading rate, and plume growth that govern the plume dynamics. This paper is organized as follows: the experimental facility and methodology used for single-phase and particle-laden plume experiments is described in Sect. 2. A non-dimensional relation for the maximum height of the plume is derived and compared with experiments in Sect. 3. Results and discussion on growth and spread of single-phase and particle-laden plume is given in Sect. 4. The paper ends with important conclusion from this research.

2 Experimental set up and methodology

2.1 Experimental facility

Laboratory experiments were conducted to study the effects of varying volume fraction (ϕ_v) of particles on the bulk parameters as a plume is growing and spreading in a stratified environment. In the present experiment two acrylic tanks were used: a cubical tank (T1) measuring 60 cm on each side and a square cross-sectional tank (T2) measuring 91 cm long by 91 cm wide by 60 cm high. Tank T1 was used for storing the lighter injection fluid having $\rho_j = 999$ kg/m^3 , and the second tank was used for creating the ambient linear stratification with varying strengths as shown in Fig. 1. The strength of the stratification is characterized by the Brunt Vaisala frequency, N. A double bucket system [33] was used for creating a linear stratification in the present study. In all the experiments, a constant depth of H = 47 cm was maintained. A portable densitometer (Anton paar DMA 35) was used to check the density in the two buckets. The linearity of the profile was checked using a Delta-Ohm (model HD 2106) conductivity probe. A typical density profile is shown in Fig. 15 (see Appendix).

2.2 Methodology and flow characteristics

A centrifugal pump, shown in Fig. 1, was used to discharge the jet fluid into the ambient linearly stratified environment using a round jet nozzle seated at the bottom of the stratifiation tank (T2). The jet nozzle was 160 mm in length with diameter $d_j = 12.7$ mm. It was made of aluminum and comprised of a diffuser, settling chamber, and a contraction

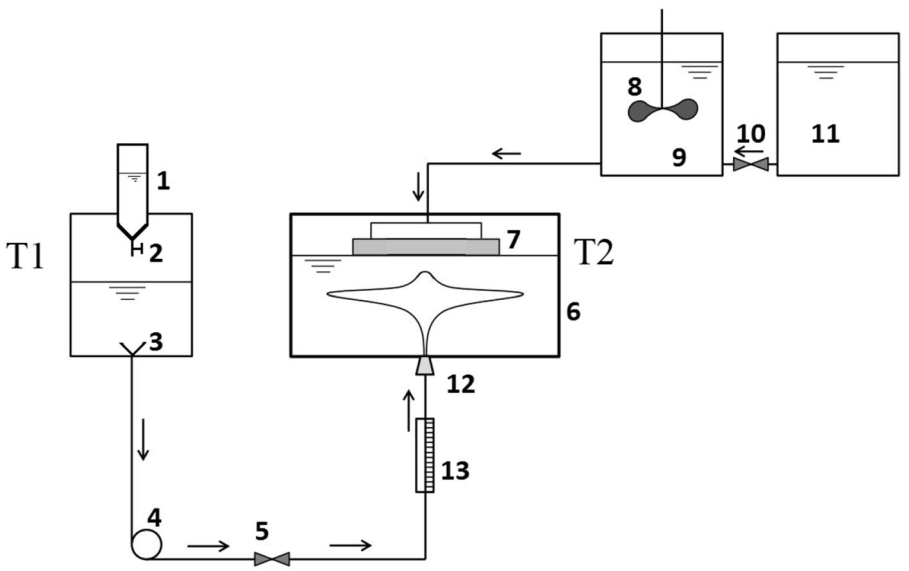

Fig. 1 Schematic of the experimental setup. *1* Conical particle feeder, *2*, *5*, *10* Control valve, *3* Funnel, *4* Centrifugal pump, *6* Stratification tank (T2), *7* Wooden plate, *8* Fluid mixer, *9* Salt water bucket, *11* Fresh water bucket, *12* Jet nozzle, *13* Flowmeter

section. It was designed based on the principle discussed by Mehta and Bradshaw for designing a wind tunnel [34]. A honeycomb was placed in the settling chamber to reduce the flow fluctuations (≈3 % in the present experiments) and to generate a stable flow at the nozzle exit. The exit vertical velocity at the nozzle was maintained constant at $W_0 = 26.3$ cm/s, thereby giving a jet Reynolds number of $Re_j = \frac{W_0 d_j}{\nu} = 3750$ and initial Richardson number of $Ri_{go} = \left(\frac{\pi}{4}\right)^{0.25} \sqrt{\frac{g' d_j}{W_0^2}} = 0.16$. The flow rate into the tank (T2) was measured using calibrated flowmeter for single phase experiments. For the particle-laden plume experiments, flow was measured by timing the decrease in the water level in the discharge tank, T1. The flow rate used in the experiments was $Q_0 \approx 33$ cm^3/s. A linear stable stratification with water and commercial salt (NaCl) was obtained in T2, such that heavy fluid settles at the bottom and lighter fluid on the top. Once the fluid is filled into tank T2 using the two-bucket system, it is allowed to stabilize for approximately 6 h to achieve stable uniform linear stratification with height.

It was observed that in all the experiments the vertical density profile was linear with an error estimate of ±0.2 % (see Fig. 15). After linear stratification is achieved in tank T2, the lighter jet fluid (dyed-water) from tank T1 is pumped into tank T2 to perform experiments to study plume dynamics. Each experimental run was repeated seven times to obtain statistically averaged measurement, and lasted between 180 and 240s. Light sources were positioned on the top and the side to improve imaging, and to ensure that shadow effects were not present.

White acrylic sheets were placed on the outer walls of the tank to diffuse the incoming light in order to obtain high quality flow visualization images. The flow dynamics were captured using a commercial dye with help of high resolution digital video camera. Two cameras, one from the side, and one from the top were fitted to record the flow dynamics in the x-z plane (side view) and x-y plane (top view). The front view of the flow evolution was recorded by a digital video camera (CANON 7D) that was positioned approximately 1m from the front wall of the tank. The top camera (NIKON D3100) was used only to check for the plume symmetry, which was confirmed from the images. The measurement data was obtained only using the front camera, and hence was devoid of any shadow effects. The horizontal and vertical spatial resolution was fixed at 0.625 mm/pixel.

The distance between the camera position and the tank was kept constant during all the experiments to ensure that the horizontal and vertical resolution (in mm/pixel) remains the same. This is important since MATLAB image processing tool was used to measure the growth, and spreading rate of the plume. Schematic representation of bulk parameters measured in the experiments is shown in Fig. 2. Here, Z_m is the maximum height of the

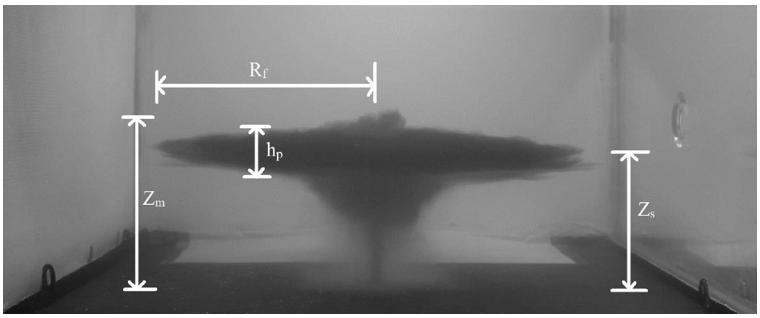

Fig. 2 Schematic representation of experimental parameters for multi-phase plume with $\phi_v = 0.5\,\%$

Table 1 Experimental run conditions and data

Run no.	d_j (cm)	N (s^{-1})	W_0 (cm)	Re	d_p (μm)	ϕ_v (%)	Ri_{go}	B_0 (m^4/s^3) × 10^{-6}	M_0 (m^4/s^2) × 10^{-6}	No. of trials (n)
1	1.27	0.67	26.3	3750	100	0	0.16	6.67	8.67	7
2	1.27	0.67	26.3	3750	100	0.35	0.16	6.67	8.67	7
3	1.27	0.67	26.3	3750	100	0.5	0.16	6.67	8.67	7
4	1.27	0.67	26.3	3750	100	0.7	0.16	6.67	8.67	7

plume, Z_s is the spreading height of plume, R_f is the radial intrusion of plume, and h_p is the plume thickness measured near start of the intrusion and during plume propagation.

The particles used in the particle-laden plume experiments were glass beads of mean diameter $d_p = 100$ μm, with density $\rho_p = 2500$ kg/m^3. The settling velocity of the particle was $w_s = \frac{g(\rho_p - \rho_b)d_p^2}{18\mu} = 8$ mms^{-1}. Three different volume fraction of particles were used, namely, $\phi_v = 0.35$, 0.5 and 0.7 %. The uncertainty involved in calculating the volume fraction, ϕ_v, is within ±1 %. These particles were injected into the pump suction using a conical particle feeder (see Fig. 1). The particles would get uniformly mixed with the fluid before ejecting out from the nozzle. In order to avoid the splashing of particles outside the suction pipe, a conical funnel was placed at the suction end of the pump. An aluminum tray placed at the bottom of stratification tank (T2) was used to collect the glass beads at the end of each experimental run. These particles were then dried to measure the exact volume fraction in the experiments. This is to ensure the particle losses that may take place inside the pipe. For all the experiments, the value of Brunt Vaisala frequency was fixed as $N = 0.67$ s^{-1}, which could be classified as moderate strength. By fixing the value of N, we varied ϕ_v to understand the effect of particles on plume dynamics. Details of the experimental runs performed are shown in Table 1. The value of $(M_0/B_0)N^{1/2} \approx 1.06$, which means that we are in the buoyant jet or forced plume regime [12].

2.3 Image processing

In this section, we discuss the methodology used to extract the data from the images. Image segmentation technique using MATLAB analysis software was used. Initially, the video recording from the digital camera was converted into images. The intensity contrast of the image was enhanced, followed by background subtraction to get the required segmented image. From this segmented image the high intensity band was selected and a threshold was applied to get the images in the binary form. From these binary images the edge coordinates were extracted for further data interpretation. The intensity cut-off for detecting the edge was set at ±5 % of the maximum value. This was to ensure that the effect of background noise on the measurement was minimum. The uncertainty involved in the image processing was within ±2 %.

3 Dimensional analysis

Based on the assumption that the entrainment of ambient fluid by the plume occurs at a rate proportional to the mean vertical velocity, and existence of self-similar vertical velocity and buoyancy profiles, Morton et al. [8] proposed an analytical expression for the

maximum height, Z_m, for a single phase plume. Due to the complex nature of vertical velocity profile in a particle-laden plume, as evident from Fig. 3, non-dimensional approach was used to construct an empirical relation for Z_m for particle-laden case. The dependent variable, Z_m, can be written as a function of the following flow variables,

$$Z_m = f(W_0, d_j, d_p, \mu, \rho_j, \rho_t, \rho_b, \rho_p, g, \phi_v, z) \tag{6}$$

where μ is the dynamic viscocity of fluid, z is the vertical distance and ρ_t is the density of the top layer fluid. The above equation can be reduced in terms of momentum flux, M_0, buoyancy flux, B_0, Brunt Vaisala frequency, N, and particle settling velocity, w_s, as shown below,

$$Z_m = f(M_0, B_0, N, w_s, \phi_v) \tag{7}$$

For a plume, as the momentum flux, M_0, is small compared to the buoyancy flux, B_0, M_0, can be neglected. So Eq. (7) reduces to,

$$Z_m = f(B_0, N, w_s, \phi_v) \tag{8}$$

From Eq. (8), we can form three π terms based on Buckingham Pi-theorem. These terms are given below,

The first π term can be written as,

$$\pi_1 = \frac{Z_m}{(B_0/N^3)^{1/4}} \tag{9}$$

which characterizes some form of a non-dimensional vertical length scale.

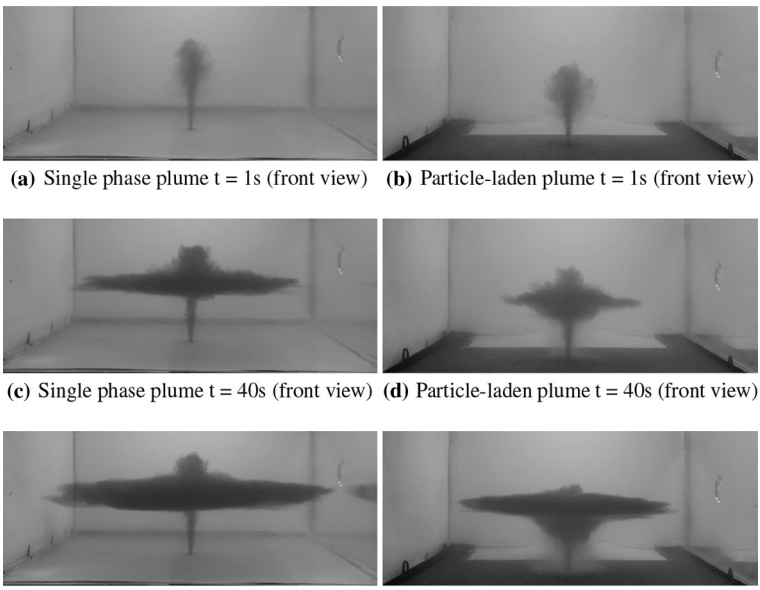

(a) Single phase plume t = 1s (front view) **(b)** Particle-laden plume t = 1s (front view)

(c) Single phase plume t = 40s (front view) **(d)** Particle-laden plume t = 40s (front view)

(e) Single phase plume t = 90s (front view) **(f)** Particle-laden plume t = 90s (front view)

Fig. 3 Snapshots of plume development for $N = 0.67$ s $^{-1}$ for case of $\phi_v = 0\,\%$ (**a**, **c**, **e**) and $\phi_v = 0.5\,\%$ (**b**, **d**, **f**)

The second term is

$$\pi_2 = \frac{w_s}{(B_0 N)^{1/4}} \tag{10}$$

which characterizes the non-dimensional velocity scale, which is the ratio of the particle velocity to the plume velocity. The term π_2 is seldom referred to as the non-dimensional slip velocity [35]. The fluid will settle along with the particle as and when the buoyancy flux vanishes.

The third term represents the particle volume fraction present in the plume,

$$\pi_3 = \phi_v \tag{11}$$

Arranging the three non-dimensional π terms approriately, we can arrive at the final form of Z_m as follows,

$$Z_m = \left[C - C_1 \left(\frac{\phi_v w_s}{(B_0 N)^{1/4}} \right) \right] (B_0/N^3)^{1/4} \tag{12}$$

The above equation makes sense because the maximum height Z_m should be lower for the particle-laden plume due to the presence of negatively buoyant particles. If we simply take the case of a single phase plume, then it is clear that only π_1 would exist, and from Buckingham Pi-theorem, it should be equal to a constant, C. In the presence of particles, additional π terms in form of π_2 and π_3 are introduced, which could be combined together to form the non-dimensional slip velocity. From physical arguments that Z_m should be lower in the presence of negatively-buoyant particles, we arrive at the final form of the empirical equation for Z_m as shown in Eq. (18), where C and C_1 are empirical constants. We would like to point out that, this equation has some similarity to the one proposed by Masutami and Adams [35] for the case of oil jet injected in a stratified medium. However, their final equation doesn't include the particle volume fraction, and was proposed for the spreading height of the plume.

4 Results and discussion on single-phase and multi-phase plume

Experiments were performed by fixing all the flow parameters except the particle volume fraction, which was varied from ϕ_v = 0–0.7 %. The condition $\phi_v = 0\,\%$ is akin to the single-phase plume case. In Fig. 3, images of plume evolution for $\phi_v = 0\,\%$ is shown, which follows a similar trend reported in the literature [8, 9]. The plume is forced out of the nozzle and rises upwards. The plume then reaches a height where the density of the plume fluid is in equilibrium with the ambient stratified fluid, and this point is called the neutral buoyant region. In this neutral buoyant region, the plume will no longer rise through buoyancy, but solely through any upward momentum that it has. This is called the umbrella region, and is usually marked by the column spreading out sideways. The upward inertia present in the plume after intruding the neutral buoyant layer results in formation of a fountain like structure on the top, which is a unique feature of single-phase plume. In Fig. 3, plume evolution for multi-phase plume, with $\phi_v = 0.5\,\%$ is also shown. On comparison, it is evidently seen that the presence of particles changes the plume evolution behavior. Three distinct differences could be documented: (i) due to the presence of particles, upward plume inertia is not sustained, hence the fountain like structure on the top

is obliterated, (ii) with time, 'particle fall out'effect occurs, and a parabolic cloud of fluid (along with dispersed particles) is seen below the neutral buoyant layer, and (iii) at later times, there is a secondary umbrella region, where the plume spreads horizontally closer to the source. 'Particle fall out'effect is defined as the fall of particles from the neutral buoyant layer due to gravity, once the particles lose their upward momentum. As the particles from the neutral buoyant layer fall down, they drag the plume along with it, and form the parabolic cloud below the neutral buoyant layer as shown in Fig. 3. The particle fall out phenomenon is partially responsible for modified dynamics of a particle-laden plume.

For both single-phase and particle-laden plume, once the plume develops, bulk characteristics were measured and plotted as a function of radial distance or time in order to understand the plume dynamics in detail. Some of the key parameters and their evolution are discussed below.

4.1 Maximum height of plume (Z_m)

The maximum height of the plume, Z_m, is defined as the distance from the source to the maximum vertical height attainable by the plume in the stratified medium. This is the most common large scale flow parameter measured in plume flows. The empirical entrainment coefficient α can be deduced by measuring Z_m. In the present experiment, the variation of Z_m with time was studied for $\phi_v = 0, 0.35, 0.5$, and $0.7\,\%$. To find Z_m, the sequence of images captured using the camera were processed using image segmentation technique discussed in Sect. 2.3.

In Fig. 4, the variation of Z_m with time is shown. This figure was obtained by ensemble averaging the number of experimental runs for each volume fraction using the following formula,

$$Z_m = \frac{1}{n}\sum_{i=1}^{n} z_m \tag{13}$$

where z_m is the instantaneous value of maximum height from the experiments, and n is the number of experimental runs. From Fig. 4, we see that during the plume development stage, the maximum height steadily increases and reaches a steady state at later times. This

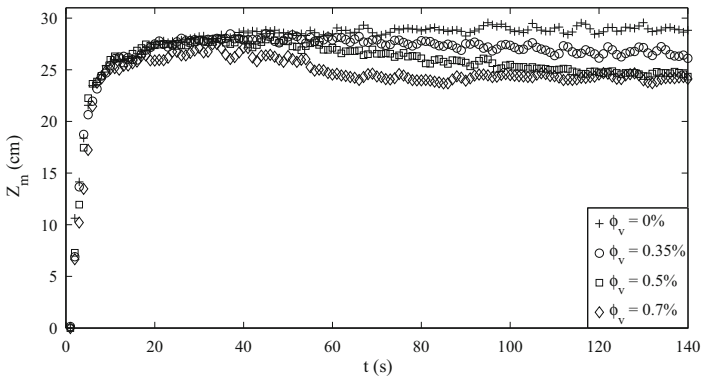

Fig. 4 Plot showing variation of maximum height of plume Z_m versus time, t

trend was observed for all the four ϕ_v used in our experiment, and is attributed to the initial transient required for the plume to reach a steady state. Once the plume reaches the steady state, the variation in Z_m about the mean value is $\pm 2\,\%$. An interesting observation is that steady state Z_m has the highest value when $\phi_v = 0\,\%$, and the value decreases with increasing ϕ_v. Such a trend is expected because, increasing the particle concentration increases the drag on the rising plume due to negative buoyancy of the particles, thereby inhibiting the vertical span achievable by the plume.

In Fig. 5, we show the variation of the mean maximum height $\overline{Z_m}$ with ϕ_v for $N = 0.67\ \mathrm{s}^{-1}$. After the flow reaches a steady state, the mean maximum height was computed by time averaging the Z_m values as follows,

$$\overline{Z_m} = \frac{1}{t - t_0} \sum_{t=t_0}^{t} Z_m \tag{14}$$

From Fig. 5, a clear decreasing trend is observed for the mean maximum height. Further, the experimental data was validated with the non-dimensional empirical expression formulated for Z_m in Sect. 3. In order to find the constant C in Eq. (12), we can invoke the single-phase Z_m expression derived by Morton et al. [8] given as follows,

$$Z_m = 0.41\ \alpha^{-1/2}\ B_0^{1/4}\ N^{-3/4}\ z_1 \tag{15}$$

Here Z_m indicates the maximum height of plume, B_0 is the initial buoyancy flux, N is the Brunt Vaisala frequency, and α is the entrainment coefficient, which is empirical, and is dependent on flow conditions. The term $z_1 = 2.8$ indicates non-dimensional height at which vertical velocity vanishes. For our present single-phase experiment for $N = 0.67\ \mathrm{s}^{-1}$, the entrainment coefficient was found to be $\alpha \approx 0.068$ based on the bulk parameter method. The entrainment coefficient for a pure plume given by Morton et al. [8] was $\alpha \approx 0.083$. The reason for the discrepancy in our present α with that given in [8] is because, as stated earlier, for our experiments $(M_0/B_0)N^{1/2} \approx 1.06$. When $0.1 < (M_0/B_0)N^{1/2} < 2$, Konstantinidou and Papanicolaou (2003) [12] proposed the following empirical formula,

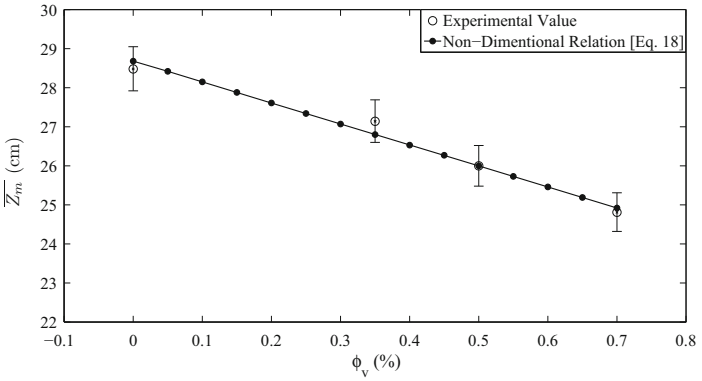

Fig. 5 Plot of the mean maximum height of plume $\overline{Z_m}$, versus volume fraction (ϕ_v). Here (*open circle*) represents experimental measurements, and (*filled circle*) represents the predictions obtained from Eq. (18)

$$\alpha = \alpha_p \; exp\left[ln\left(\frac{0.025}{\alpha_p}\right)\left(\frac{(M_0/B_0)N^{1/2}}{2}\right)^2\right] \tag{16}$$

Based on this empirical formula, the value of α comes out to be $\alpha \approx 0.06$, which is in close agreement with the α obtained for our present study. As already discussed in Sect. 1, α is not a self-similar parameter and has a strong correlation with the experimental conditions. Moreover, in our experiments α was calculated based on bulk parameter, Z_m, and hence the value given here is lower than that predicted by Morton et al. [8]. Based on $\alpha = 0.068$, Eq. (15) becomes,

$$Z_m = 4.4 \; B_0^{1/4} \; N^{-3/4} \tag{17}$$

Combining Eqs. (12) and (17), we can write a generalized empirical relation for particle-laden plume as

$$Z_m = \left[4.4 - 450\left(\frac{\phi_v w_s}{(B_0 N)^{1/4}}\right)\right](B_0/N^3)^{1/4} \tag{18}$$

where, the constants C and C_1 in Eq. (12) are empirical and obtained from experimental measurements. The value of constant C was first given by Morton et al. [8] and lies between C = 3.98 and 5 depending on the plume flow condition. When $\phi_v = 0\,\%$, the above expression reduces to Eq. (17) for the single-phase plume. The experimental maximum height of the plume was then compared with Eq. (18). As shown in Fig. 5 a satisfactory match is obtained between the experimental and the empirical Z_m calculated using Eq. (18).

4.2 Spreading height of plume

The spreading height of the plume, Z_s, is defined as the mean height of the plume from the source, when it starts intruding in the horizontal direction at the neutral buoyant layer. In order to find the Z_s, image segmentation technique was used as discussed in Sect. 2.3. From the images, Z_s was found by taking the vertical distance from the source to the mean of plume thickness (see Fig. 2). The spreading height follows the same trend as that of the

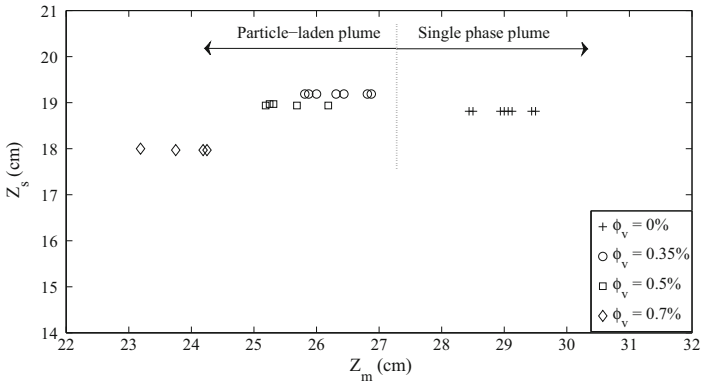

Fig. 6 Spreading height, Z_s, plotted against the maximum height, Z_m for single-phase plume and particle-laden plume

maximum height, Z_m, but Z_s is always smaller than Z_m. The variation of Z_s versus Z_m is shown in Fig. 6. From this figure, it is seen that the value of Z_s/Z_m for the single-phase plume is $Z_s/Z_m \approx 0.68$, consistent with the measurements by Richards et al. [9]. For the particle-laden plume $Z_s/Z_m \approx 0.75$. This increase in the ratio of Z_s/Z_m could be attributed to the fact that the particles reduce the buoyancy flux in the plume, which inturn inhibits the maximum height of the plume, thereby increasing the value of Z_s/Z_m. It was also observed that in the case of particle-laden plume, increasing the volume fraction of the particles decreases the value of Z_s. To elaborate, for the particle-laden plume, Z_s was found to be similar to the single-phase case at very low $\phi_v \approx 0.35$ and 0.5 %. For $\phi_v = 0.7\%$ a significant decrease in the value of Z_s was seen. Hence, it could be concluded that beyond a critical value of ϕ_v, the spreading height starts intruding the neutral buoyant layer much closer to the source. This could be due to the 'particle fall out' effect, which has been described earlier. The particles which are initially flown along with jet momentum tend to fall due to the gravity once they lose their momentum. The falling particles are re-entrained into the plume, thereby reversing the buoyancy (i.e. cause a negative buoyant effect) of the uprising plume. This causes partial plume collapse and decreases the maximum height of the plume, Z_m, as well as the spreading height, Z_s. The particle fall out effect becomes important at high particle loading as seen from Fig. 6. Therefore, for plume with $\phi_v = 0.7\,\%$, the Z_m and Z_s values were found to be much lower than for the single-phase case.

4.3 Radial intrusion of plume

Radial intrusion of plume (R_f) in a linear stratified medium was studied for both single-phase and particle-laden plume. To measure R_f, image segmentation technique was used as discussed in Sect. 2.3. The co-ordinates of the segmented images were extracted to form $R_f(t)$. The results of plume spread for different values of volume fraction, ϕ_v, is shown in Fig. 7. We observed from the experiments that particle-laden plume follows four different growth regimes, namely, (i) radial momentum balanced by the inertia force, (ii) inertia buoyancy regime, (iii) fluid-particle inertia regime, and (iv) viscous buoyancy regime. It was also observed that regime (iii) was absent for the case of single-phase plume which is consistent with previous studies [9, 17]. Below we discuss each region in detail.

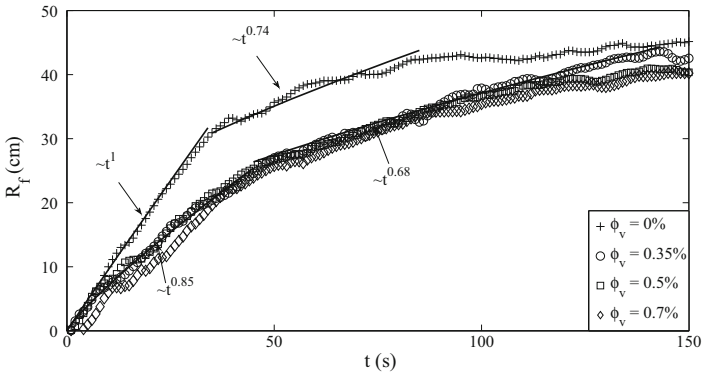

Fig. 7 Radial distance, R_f, of the intrusion front from the plume centerline as a function of time

4.3.1 Regime I

Radial momentum balanced by inertia This regime is observed as soon as the plume becomes neutrally buoyant and starts to spread radially outward. The momentum associated with the plume allows an initial faster plume growth. In the single-phase plume, in this regime, the radial front, R_f, grows linearly with time for $t \leq 30$ s as seen in Fig. 7. In the case of particle-laden plume, R_f, follows a power law, where $R_f \propto t^{0.85}$ for $t \leq 30$ s.

4.3.2 Regime II

Inertia buoyancy regime This is an important regime in which the plume spreads primarily due to the buoyancy effects. Once the plume reaches the neutral buoyant level, the plume intrudes horizontally due to inertia. The vertical spread is due to the buoyancy effects arising from small density differences between the plume fluid and the ambient fluid that is present below the spreading height. The density difference is a result of the entrainment process occuring below the spreading height. The plume spread in this region is referred to as "coning", and is a typical characteristic of neutral conditions where the plume moves radially outward forming an umbrella cloud. Following the plume development ($t \approx 30$ s), the plume propagates at a lower speed as seen from Fig. 7, where $R_f \propto t^{0.74\pm0.02}$ ($30 \text{ s} \leq t \leq 85 \text{ s}$) for single phase case, and $R_f \propto t^{0.68\pm0.02}$ ($30 \text{ s} \leq t \leq 130 \text{ s}$) for $\phi_v > 0$. The spread rate, R_f, for single-phase case in our experiments was similar to that observed by previous researchers who obtained $R_f \propto t^{0.75}$ [36, 9]. Therefore, from our results it could be concluded that the radial propagation of particle-laden plume is slower than that of single-phase case. When the particle-laden plume intrudes into neutral buoyant layer the particles follow the flow to a certain distance after which the 'particle fall out' effect occurs resulting in reduced buoyancy flux, and slow propagation of the plume front.

4.3.3 Regime III

Fluid-particle inertia regime This regime is only observed when $\phi_v > 0\,\%$. For a particle-laden plume, the fluid affects the particle, and the particle in turn affects the fluid, commonly referred to as two-way coupling [22]. The two-way coupling mechanism is important when the volume fraction of particle, ϕ_v, lies between $10^{-6} < \phi_v < 10^{-2}$, which is the case in our present study. This implies that the particle dynamics, and its inertia can have considerable effect on the plume behavior. This effect is clearly seen in Figs. 7, 8. In Fig. 7, as ϕ_v increases from 0.35 to 0.7 %, we observe that the fluid-particle inertia regime is delayed, preceded by a longer inertia-buoyancy regime. For the case when ϕ_v= 0.35 %, the fluid-particle inertia regime is enountered close to $t \approx 140$ s, whereas for ϕ_v= 0.7 %, this regime is encountered earlier at $t \approx 110$ s. The transition to fluid-particle inertia regime in Fig. 7 is seen as lowering of plume radial propagation speed from $t^{0.68}$, which occurs earlier for $\phi_v = 0.7$ %.

The effect of particles on plume dynamics is also qualitatively seen in Fig. 8, where the radial plume propagation is shown at one single time, $t = 120$ s. It is seen that as the particle volume fraction increases, the radial propagation of the plume slows down. At time, $t \approx 120$ s, for $\phi_v = 0.35\,\%$, the particles seem to have little effect on the plume dynamics compared to $\phi_v = 0.7\,\%$, where a plume column is distinctly seen. Moreover, in Fig. 8, a weak secondary umbrella cloud formation is observed for $\phi_v = 0.7\,\%$, which could play a role in the reduction of the plume radial speed after $t \geq 120$ s. The secondary

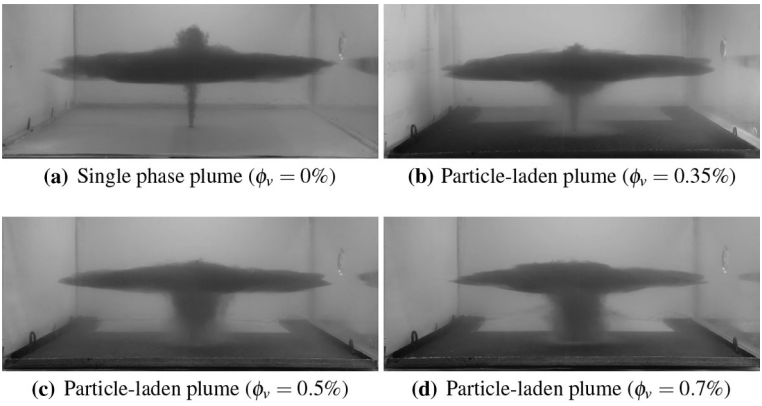

(a) Single phase plume ($\phi_v = 0\%$) **(b)** Particle-laden plume ($\phi_v = 0.35\%$)

(c) Particle-laden plume ($\phi_v = 0.5\%$) **(d)** Particle-laden plume ($\phi_v = 0.7\%$)

Fig. 8 Images showing fluid particle inertia regime for four different values of ϕ_v at time t = 120 s

Fig. 9 Secondary umbrella cloud formation for $\phi_v = 0.7\,\%$ at time $t = 150$ s

umbrella cloud is marked by the peeling of the plume at different heights due to the presence of particles. Such a secondary umbrella formation was also observed by Masutami and Adams [35] in their oil–gas jet experiments. The complete physical understanding for the secondary umbrella requires resolved measurements, and is not within the scope of the present work.

As we lower the volume fraction ($\phi_v = 0.35\,\%$), the formation of this secondary umbrella cloud is delayed and hence the inertia buoyancy regime persists for a longer time. In addition to the 'particle fall out' effect described earlier, the formation of the secondary umbrella region could also be attributed as a reason for the slow radial propagation in particle-laden plume. To clearly confirm the presence of a secondary plume, a plume image at a later time ($t \approx 150$ s) is shown for $\phi_v = 0.7\,\%$ in Fig. 9, where the secondary umbrella cloud is distinct. The fluid-particle inertia regime was observed in all our experiments for a particle-laden plume, and therefore the above explanation is consistent with the observed dynamics.

4.3.4 Regime IV

Viscous buoyancy regime In the case of viscous buoyancy regime, viscous forces dominate the plume due to the presence of wall in our experiments. For single-phase plume, due to

faster propagation of the plume in the inertia buoyancy regime, the viscous buoyancy regime was encountered earlier (85 s $\leq t \leq$ 160 s). Due to viscosity, the radial spread follows $R_f \propto t^{0.32\pm0.02}$ as seen from Fig. 7. For particle-laden plumes, the viscous buoyancy regime is encountered at a later time because of slower propagation in the inertia buoyancy regime, and due to the presence of an additional fluid-particle inertia regime as discussed above. For $\phi_v > 0\,\%$, in the viscous buoyancy regime, the plume spreads as $R_f \propto t^{0.2\pm0.02}$. It should also be noted here that, for $\phi_v > 0.7\,\%$, the viscous buoyancy regime is not seen in Fig. 7, because the plume didn't reach the wall for the time scale of our experiment. This was confirmed from Fig. 8.

4.4 Plume thickness

In this section, variation of the plume thickness (h_p) with time in two different regime was studied. The thickness was measured at different radial locations as the plume spreads horizontally. When the radial momentum of the plume balances the inertia force (regime I), the thickness of plume was plotted, and the results are shown in Fig 10. In this region, the plume thickness increases and reaches a steady value for all volume fractions. The steady state plume thickness for $\phi_v = 0$ %is $h_p = 10.5 \pm 0.5$ cm. A similar result was observed by Richards et al. [9] in their work on single-phase plume. This point was denoted as R_1 by Richards et al. [9], where R_1 is defined as the start of inertia-buoyancy regime. For consistency we will use this same notation.

In the case of particle-laden plume, we observed the same characteristics as that of single-phase plume, but with a slight decrease in the constant value $h_p \approx 8.5 \pm 0.5$ cm at point R_1. Surprisingly, this value was almost same ($\pm$0.5 %) for all the three volume fractions (ϕ_v = 0.35, 0.5 and 0.7 %).

Considering a point further away from R_1, i.e. at a radial distance of r = 12.5 cm from R_1, it was found that the plume thickness, h_p, never reached a steady value. This is shown in Fig. 11, where we observe that h_p increases with time. The rate of increase in the plume thickness seemed to follow a power law: for $\phi_v = 0$ %, $h_p \propto t^{0.45\pm0.02}$ and for $\phi_v > 0$ %, $h_p \propto t^{0.38\pm0.02}$.

The thickness of the intrusion layer was measured as a function of radial distance for different times, and is shown in Figs. 12, 13, 14. The intrusion thickness, $h_p(r,t)$ was determined from the front-view snapshots for the experimental run shown in Fig. 3. The

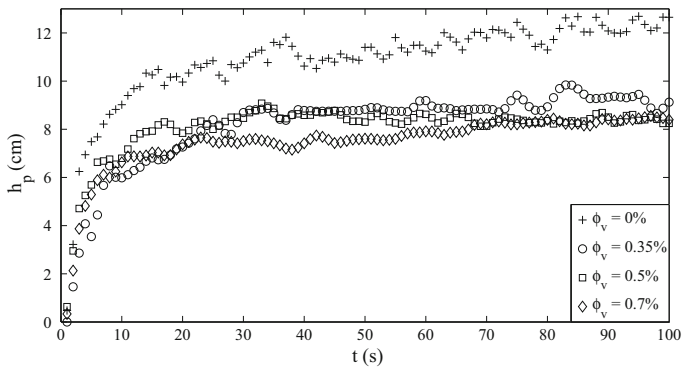

Fig. 10 Plot of the intrusion thickness (position R_1) versus time

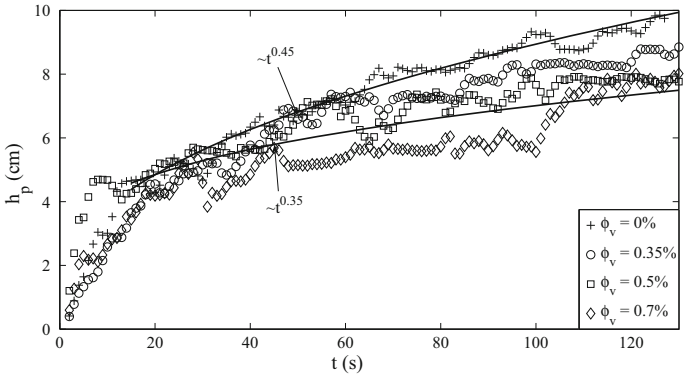

Fig. 11 Plot of the intrusion thickness versus time at a radial distance r = 12.5 cm from R_1

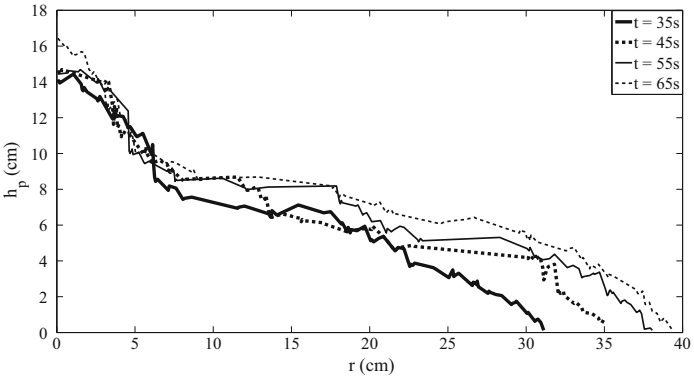

Fig. 12 Plot of the intrusion thickness, h_p, as a function of radial distance, r, for times t = 35, 45, 55, 65 s ($\phi_v = 0\,\%$)

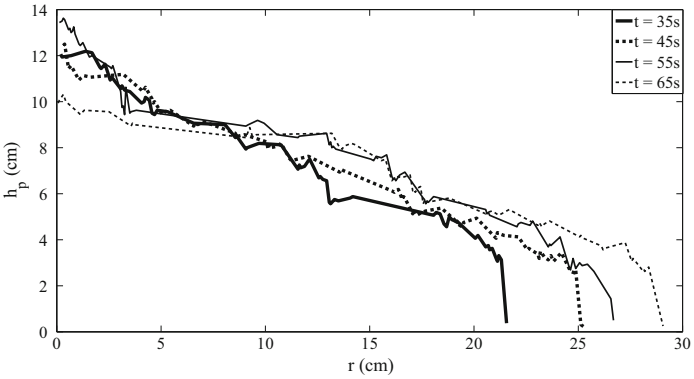

Fig. 13 Plot of the intrusion thickness, h_p, as a function of radial distance, r, for times t = 35, 45, 55, 65 s ($\phi_v = 0.5\,\%$)

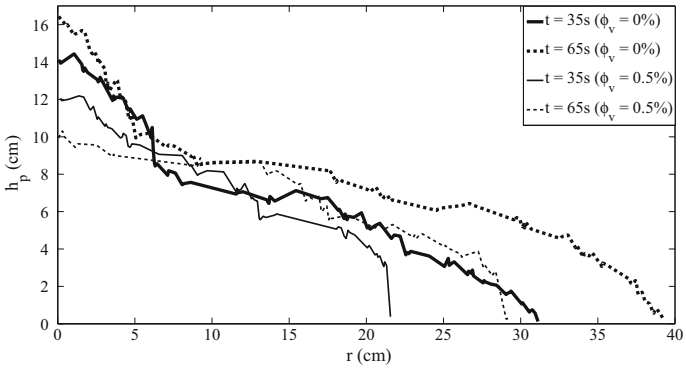

Fig. 14 Plot of the intrusion thickness, h_p, as a function of radial distance, r

profiles are plotted only for times t = 35, 45, 55, 65 s. Generally, we found that for both single-phase and particle-laden case, consistent with Fig. 10, the plume thickness remained unchanged at R_1. However, at a distance further away from R_1, the plume thickness at different times had varying values for both single-phase and particle-laden case, consistent with Fig. 11. The novel observation in the case of particle-laden plume was that, at any particular time t, the growth/thickness of the plume was found to be slower/ lesser compared to the single-phase plume, as seen from Fig. 14. We believe that the reason for the thickness of the plume being lower for multiphase case is due to the 'particle fall out' effect near the centerline of the plume, which leads to the formation of a particle cloud along with a plume column that is not observed in the single-phase case. This along with the formation of the secondary umbrella cloud could lower the plume thickness in particle-laden plumes. The exact physical reasoning for this behavior of plume thickness needs to be studied in detailed, and is scope for future work.

4.5 Theory for radial intrusion in particle-laden plume

To derive the analytical expression for intrusion front, a previously proposed box-model approach was used [37]. The speed, v_f, of the intrusion front with constant thickness, h_p, in linearly stratified fluid is given by

$$v_f = \frac{Nh_p}{\sqrt{Ri}} \tag{19}$$

Assuming no entrainment into the intrusion, the volume of the intrusion should increase in time as follows [9]

$$Q_i = 2\pi(R_f - R_1)h_p v_f \tag{20}$$

Here $Q_i \approx 2R_1 h_1 u_1$ is the volume flux of the source emanating from a radius, R_1 defined as start of inertia buoyancy regime with speed u_1 and thickness, h_1. Using this in Eq. (19) to eliminate h_p, the resulting equation for the advancement of the intrusion front becomes

$$\frac{dR_f}{dt} = v_f = \left(\frac{1}{R_i}\right)^{1/4} \left(\frac{Q_i N}{2\pi}\right)^{1/2} (R_f - R_1)^{-1/2} \tag{21}$$

Substituting and differentiating, we get,

$$R_f - R_1 \approx \left(\frac{3}{2}\right)^{2/3} \left(\frac{1}{R_i}\right)^{1/6} \left(\frac{Q_i}{2\pi N}\right)^{1/3} \left[N(t - t_1)\right]^{2/3} \tag{22}$$

This expression can be written in terms of the buoyancy flux, B_0, at R_1 through the relation

$$B_0 = Q_i g' = Q_i N^2 h_1 \tag{23}$$

This can be written for particle laden plume by introducing ϕ_v, volume fraction of particles.

$$R_f \approx \left(\frac{3}{2}\right)^{2/3} \left(\frac{1}{R_i}\right)^{1/6} \left(\frac{(1 - \phi_v) B_0}{2\pi h_1 N^3}\right)^{1/3} \left[N(t - t_1)\right]^{2/3} \tag{24}$$

Our experimental results shows that $R_f \propto t^{2/3}$ for particle laden case which matches with the model assuming constant volume flux with no entrainment. Another approach based on constant buoyancy flux was used by Richards et al. [9], where entrainment was taken into account. The constant buoyancy model gave $R_f \propto t^{3/4}$ [9]. At this point, it is not clear whether constant volume approach is suitable for validation of R_f for particle laden plume. This is scope for future work.

Comparing our experimental results on radial spreading rate with field observation presents a very interesting correlation in the Pinatubo plume spread [38], where the radius increased as $t^{0.65\pm0.01}$ for distances upto 600 km. This power law observation was consistent with our particle-laden experiments. In the case of single-phase plume, intrusion radius increases as $R_f \approx t^{0.75\pm0.02}$. From the above observations, we could conclude that the presence of particles could modify the plume behavior as evidenced from the Pinatubo plume spread.

5 Conclusion

This paper presents the results of dispersed particle-laden plume in linearly stratified medium. With the help of laboratory experiments and theoretical parameterization, we studied the effect of dispersed particles on the bulk parameters like maximum height (Z_m), spreading height (Z_s), radial intrusion, (R_f) and thickness (h_p) of the plume. It was found that Z_m in case of particle-laden plume decreases with increasing ϕ_v. For particle-laden plume, Z_s/Z_m was found to be higher compared to single-phase plume. Such a behavior could be tied to the fact that the presence of particles decrease the buoyancy flux, which inturn decreases Z_m, and thereby increases Z_s/Z_m. The values of Z_s/Z_m in the single-phase plume were found to be consistent with other experiments [9]. The mean maximum height, $\overline{Z_m}$ in the single-phase plume was found to be higher compared to particle-laden plume. This was validated with the empirical relation that was formulated based on dimensional analysis. The reason for the reduction in $\overline{Z_m}$ for particle-laden plume is because of the 'particle fall out' effect.

The radial intrusion, $R_f \propto t^{0.74\pm0.02}$ for the single phase plume ($\phi_v = 0\,\%$) in inertia-buoyancy regime, which was observed in other experiments [36, 9]. In particle-laden plume, R_f was found to change as $t^{0.68\pm0.02}$. This was confirmed with an analytical expression developed using constant volume flux without any entrainment. For the case of particle-laden plume, another regime, termed as fluid-particle inertia regime, was noted. In this regime due to the two-way coupling between the plume fluid and particles, the dynamics of radial propagation changes, and a secondary umbrella cloud is observed that is typical of such particle-laden flows.

The variation of plume thickness, h_p, with time, at a particular radial position, was measured for both single-phase and particle-laden plume. In regime I, initially, h_p was found to increase with time, and thereafter it remained at a steady constant value. This radial distance was denoted as R_1, and at this point the thickness of the plume doesn't change for both single-phase and particle-laden plume. The location R_1 corresponds to the start of the inertia-buoyancy regime. Considering a location away from R_1, h_p increases with time in accordance with $t^{0.45\pm0.02}$ for single-phase plume, and as $t^{0.38\pm0.02}$ for particle-laden plume. The growth in h_p with time was observed only in the inertia-buoyancy regime (regime II). We also measured the variation of h_p with radial distance and found that though the thickness of plume decreases with increasing radius for both the single-phase and particle-laden plume. Also, at a given radius, R, the plume thickness, h_p, was found to be lower for the particle-laden plume. This lower value of h_p in particle-laden case could be attributed to the 'particle fall out' effect, and to the formation of secondary umbrella.

Acknowledgments The authors acknowledge funding from Indian Institute of Technology Bombay and Ministry of Earth Sciences for the present research work.

Appendix

The density profile measured using the conductivity probe in the stratified tank (T2) is shown in Fig. 15.

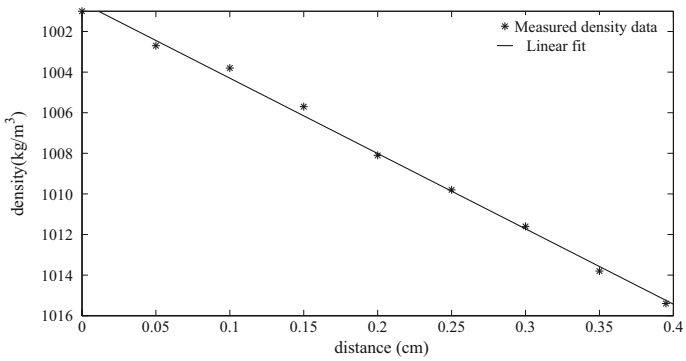

Fig. 15 Density profile in the stratification tank measured using the conductivity probe

References

1. Fernando HJS (1991) Turbulent mixing in stratified fluids. Annu Rev Fluid Mech 23:455–493
2. Linden PF (1979) Mixing in stratified fluids. Geophys Astrophys Fluid Dyn 13(1):2–23
3. Peltier WR, Caulfield CP (2003) Mixing efficiency in stratified shear flows. Annu Rev Fluid Mech 35:135–167
4. Camilli R, Reddy CM, Yoerger DR, Van Mooy BAS, Jakuba MV, Kinsey JC, McIntyre CP, Sylva SP, Maloney JV (2010) Tracking hydrocarbon plume transport and biodegradation at deepwater horizon. Science 330(6001):201–204
5. Ai J, Law AWK, Yu SCM (2006) On boussinesq and non-boussinesq starting forced plumes. J Fluid Mech 558:357–386
6. Turner JS (1986) Turbulent entrainment: the development of the entrainment assumption, and its application to geophysical flows. J Fluid Mech 173:431–471
7. List EJ (1982) Turbulent jets and plumes. Annu Rev Fluid Mech 14:189–212
8. Morton BR, Taylor GI, Turner JS (1956) Turbulent gravitational gonvection from maintained and instantaneous sources. Proc R Soc Lond A 234(1196):1–23
9. Richards TS, Aubourg Q, Sutherland BR (2014) Radial intrusions from turbulent plumes in uniform stratification. Phys Fluids 26(3):036602
10. Schmidt W (1941) Turbulente ausbreitung eines stromes erhitzter luft. ZAMM—J Appl Math Mech 21(6):351–363
11. Morton BR (1959) Forced plumes. J Fluid Mech 01:151–163
12. Konstantinidou K, Papanicolaou PN (2003) Vertical round and orthogonal buoyant jets in a linear density-stratified fluid. In: Ganoulis J & Prinos P (eds.) proceedings XXX IAHR Congress on water engineering and research in a learning society: modern developments and traditional concepts , Inland Waters: Research, Engineering and Management Theme, (theme C Nezu I & Kotsovinos N (eds.)) 1:293–300
13. Kaye NB, Linden PF (2004) Coalescing axisymmetric turbulent plumes. J Fluid Mech 502:41–63
14. Mott Richard W, Woods AW (2009) On the mixing of a confined stratified fluid by a turbulent buoyant plume. J Fluid Mech 623:149–165
15. Duo X, Chen J (2012) Experimental study of stratified jet by simultaneous measurements of velocity and density fields. Exp Fluids 53(1):145–162
16. Adalsteinsson DD et al. (2011) Subsurface trapping of oil plumes in stratification: laboratory investigations. A Record-Breaking Enterprise, Monitoring and Modeling the Deepwater Horizon Oil Spill, pp. 257–262
17. Rooney GG, Devenish BJ (2014) Plume rise and spread in a linearly stratified environment. Geophys Astrophys Fluid Dyn 108(2):168–190
18. Socolofsky SA, Adams EE (2002) Multi-phase plumes in uniform and stratified crossflow. J Hydraul Res 40(6):661–672
19. Chou Y-J, Fringer Oliver B (2008) Modeling dilute sediment suspension using large-eddy simulation with a dynamic mixed model. Phys Fluids 20(115):103
20. Wang R-Q, Law AWK, Adams EE, Fringer OB (2011) Large-eddy simulation of starting buoyant jets. Environ Fluid Mech 11(6):591–609
21. Yuan LL, Street RL, Ferziger JH (1999) Large-eddy simulations of a round jet in crossflow. J Fluid Mech 379:71–104
22. Balachandar S, Eaton JK (2010) Turbulent dispersed multiphase flow. Annu Rev Fluid Mech 42:111–133
23. Balasubramanian S, Voropayev SI, Fernando HJS (2008) Grain sorting and decay of sand ripples under oscillatory flow and turbulence. J Turbul 9(17):1–19
24. Leah SR (1994) An experimental comparison of bubble and sediment plumes in stratified environments. Dept. of Civil and Environmental Engineering, M.s., Massachusetts Institute of Technology
25. Cardoso Silvana SS, Zarrebini Mehrān (2001) Sedimentation of polydispersed particles from a turbulent plume. Chem Eng Sci 56(16):4725–4736
26. Mehrãn Z, Cardoso SSS (2000) Patterns of sedimentation from surface currents generated by turbulent plumes. AIChE J 46(10):1947–1956
27. Ernst GGJ et al (1996) Sedimentation from turbulent jets and plumes. J Geophys Res: Solid Earth 101(B3):5575–5589
28. Carey SN, Sigurdsson H, Sparks RSJ (1988) Experimental studies of particle-laden plumes. J Geophys Res: Solid Earth 93(B12):15314–15328
29. Graham V, Woods AW (2002) Particle recycling in volcanic plumes. Bull Volcanol 64(1):31–39

30. Chow AC (2004) Effects of buoyancy source composition on multiphase plume behavior in stratification. Dept. of Civil and Environmental Engineering, M.s., Massachusetts Institute of Technology
31. Chan GKY (2013) Effects of droplet size on intrusion of sub-surface oil spills. Dept. of Civil and Environmental Engineering, M.s., Massachusetts Institute of Technology
32. Jessop D, Jellinek M (2013) The effect of fine particles on ash cloud and plume dynamics. AGU Fall, Meeting Abstracts p C2860
33. Oster G, Yamamoto M (1963) Density gradient techniques. Chem Rev 63(3):257–268
34. Mehta RD, Bradshaw P (1979) Design rules for small low-speed wind tunnels. Aeronaut J 83(827):443–449
35. Masutami SM, Adams EE (2004) Experimental study of multi-phase plumes with application to deep ocean oil spills. In: Technical report, U.S. Department of the Interior, Minerals Management Service
36. Kotsovinos N (2000) Axisymmetric submerged intrusion in stratified fluid. J Hydraul Eng 126(6):446–456
37. Huppert HE, Simpson JE (1980) The slumping of gravity currents. J Fluid Mech 99:785–799
38. Holasek RE, Self S, Woods AW (1996) Satellite observations and interpretation of the 1991 mount pinatubo eruption plumes. J Geophys Res: Solid Earth 101(B12):27635–27655